ACKNOWLEDGMENTS

The author would like to thank Professor K. Nishijima for stimulating discussions, without which this work could not have been done. He is grateful to Professor J. D. Jackson for valuable comments and to Dr. R. L. Schult for a careful reading of the manuscript. He would also like to express his sincere thanks to the Fulbright Commission for a travel grant.

PHYSICAL REVIEW VOLUME 132, NUMBER 1 1 OCTOBER 1963

Scattering of 300-MeV Positrons from Cobalt and Bismuth*

J. GOLDEMBERG, J. PINE,† AND D. YOUNT‡
High-Energy Physics Laboratory, Stanford University, Stanford, California
(Received 16 May 1963)

Positrons and electrons from the Stanford Mark III linear accelerator have been scattered from cobalt and bismuth at 300 MeV. The ratio R, equal to $(\sigma_-{-}\sigma_+)/(\sigma_-{+}\sigma_+)$, has been measured at a number of angles from 10° to 45° for cobalt and from 5° to 45° for bismuth. Two experiments are reported: a high-percision experiment with poor energy resolution, suitable for measuring the small values of R found at small angles, where inelastic scattering is not important; and an experiment with somewhat lower precision but better energy resolution, suitable for measuring the larger values of R found at angles where inelastic scattering must be taken into account. The elastic scattering data are in good agreement with phase-shift calculations of Herman, Clark, and Ravenhall, who used nuclear charge distributions which fit earlier electron scattering data. The inelastic data, for which no reliable predictions exist, indicate that $R_{\text{inelastic}}$ is generally smaller than R_{elastic}. This suggests that the inelastic scattering is better described by the first Born approximation, in which $R=0$, than is the elastic scattering.

INTRODUCTION

THE elastic scattering of positrons by nuclei differs from that of electrons. For point nuclei with no magnetic moment, Feshbach[1] has computed σ_+/σ_-, the ratio of positron to electron cross sections, at a given angle and energy. For backward scattering by high-Z nuclei, this ratio is $\approx 1/5$ and it approaches 1 as the scattering angle and the atomic number are made small. The effect can be understood in terms of different spin-orbit interactions arising from the different classical trajectories of positrons and electrons scattered through the same angle. Alternatively, the effect can be ascribed to different distortions of the incident and of the scattered waves by the Coulomb field of the nucleus. In the first Born approximation, which takes into account only 1-photon exchanges, such distortions are neglected, and positron and electron scattering are identical. The difference in scattering is, thus, a measure of the importance of the exchange of two or more photons.

For finite nuclei, the difference between positron and electron scattering is sensitive to the distribution of nuclear charge. Figure 1 shows qualitatively the expected behavior of the difference in positron and electron scattering as a function of the scattering angle θ for fixed and equal incident energies. The difference is characterized by the quantity R, defined by

$$R=(\sigma_-{-}\sigma_+)/(\sigma_-{+}\sigma_+)\,, \tag{1}$$

where σ_- and σ_+ are the differential scattering cross sections for electrons and positrons. The initial increase of R corresponds to the point nucleus behavior. At angles where the classical trajectories begin to penetrate the nuclear charge distribution, R becomes negative. In terms of the classical trajectories, the deeper penetration of electrons into the charge distribution causes the electron cross section to become smaller than the positron cross section. Finally, as the angle is further increased, R oscillates. The de Broglie wavelengths of the positrons and electrons differ at the nucleus, and

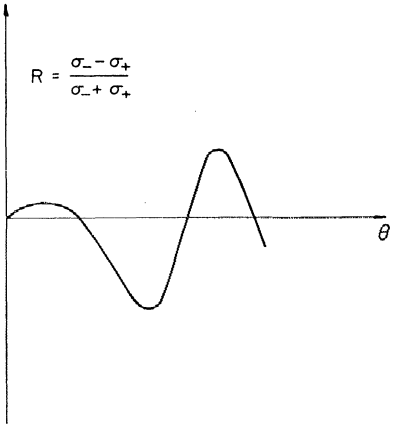

FIG. 1. Qualitative behavior of the ratio R as a function of scattering angle for nuclei of finite size.

* This work was supported in part by the U. S. Office of Naval Research, the U. S. Atomic Energy Commission, and the U. S. Air Force Office of Scientific Research.
† Present address: California Institute of Technology, Pasadena, California.
‡ Present address: Department of Physics, Princeton University, Princeton, New Jersey.
[1] H. Feshbach, Phys. Rev. 88, 295 (1952).

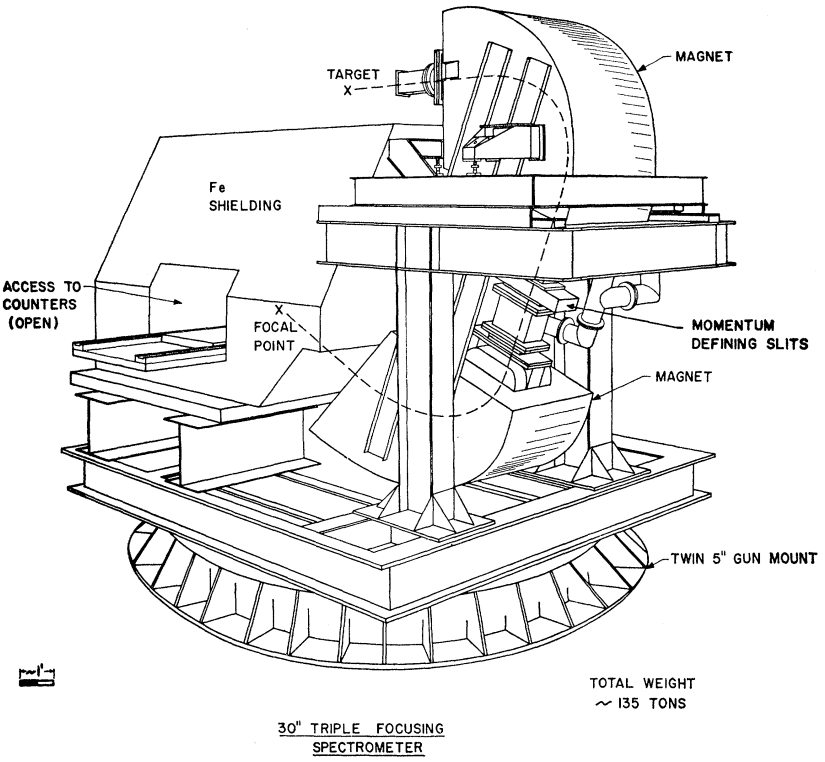

FIG. 2. Perspective drawing of the double-focusing, zero-dispersion spectrometer. For the "low-resolution" experiment, the counters were at the focal point; for the "high-resolution" measurements, a "counter ladder" was located in the position of the momentum-defining slits.

hence the diffraction minima occur at different angles. The oscillation of R reflects this effect.

The qualitative behavior shown in Fig. 1 is predicted by phase-shift calculations of the elastic scattering,[2,3] and is verified by our measurements. These experiments were undertaken to measure values of R which could be compared with predictions from the nuclear charge distributions which fit electron scattering measurements. The nuclei, Co^{59} and Bi^{209}, for which quite extensive electron scattering data exist,[4–7] were chosen as representative of medium and high Z targets.

Many previous measurements of positron scattering have been made, mostly at low energies. Miller and Robinson[8] have made measurements which show nuclear size effects, and these authors summarize the previous work. Until recently, however, the extent of such studies has been severely limited. The positron beam now available from the Stanford Mark III linear accelerator has made possible a program of scope almost comparable to the electron scattering studies. The present experiments represents a preliminary investigation of the possibilities of this technique.

Inelastic scattering of positrons by nuclear levels also has considerable interest since, in analyzing similar scattering of electrons, experimenters have had to depend upon the first Born approximation in assigning multipolarities and radiation widths to the nuclear levels investigated.[6,9,10] Again, Co^{59} and Bi^{209} are convenient for a study of positron scattering since they are known to have prominent levels excited by electron scattering.

APPARATUS

Figure 2 shows the double-focusing, zero-dispersion, spectrometer which was used. While this two-magnet system, described in detail by Alvarez *et al.*,[11] is nondispersive, there is a dispersive radial focus in the plane of the momentum defining slits placed between the magnets.

The positron beam was produced in the manner that has been described previously.[12]

Scattering from the cobalt and bismuth targets was studied in two experiments utilizing somewhat different techniques. In the first experiment, the measurements were made almost exactly as described in an earlier paper on positron scattering from hydrogen.[13] The 300

[2] G. H. Rawitscher and C. R. Fischer, Phys. Rev. **122**, 1330 (1961).
[3] R. Herman, B. C. Clark, and D. G. Ravenhall, following paper, Phys. Rev. **131**, 414 (1963).
[4] B. Hahn, D. G. Ravenhall, and R. Hofstadter, Phys. Rev. **101**, 1131 (1956).
[5] H. Crannell, R. Helm, H. Kendall, J. Oeser, and M. Yearian, Phys. Rev. **121**, 283 (1961).
[6] H. Crannell, R. Helm, H. Kendall, J. Oeser, and M. Yearian, Phys. Rev. **123**, 923 (1961).
[7] H. Kendall (private communication).
[8] R. C. Miller and C. S. Robinson, Ann. Phys. (N. Y.) **2**, 129 (1957).
[9] J. H. Fregeau, Phys. Rev. **104**, 225 (1956).
[10] R. H. Helm, Phys. Rev. **104**, 1466 (1956).
[11] R. A. Alvarez, K. L. Brown, W. K. H. Panofsky, and C. T. Rockhold, Rev. Sci. Instr. **31**, 556 (1960).
[12] D. Yount and J. Pine, Nucl. Instr. Methods **15**, 45 (1962).
[13] D. Yount and J. Pine, Phys. Rev. **128**, 1842 (1962).

MeV incident beams had momentum spreads of $\pm 1\%$; the momentum slit of the spectrometer was set at $\Delta p/p = 7\%$; the scattered positrons or electrons were detected in a two-scintillator telescope at the focus of the spectrometer; and the beam was monitored with two hydrogen-filled ion chambers and a Faraday cup. The data were taken with frequent changes from right to left scattering angle to minimize sensitivity to the beam direction, and the beam position was monitored with a split-plate ion chamber, also described in Ref. 13. The only difference, other than the target materials, was that, for the cobalt and bismuth experiment, the ion chambers were placed ahead of the target rather than behind it. This was done to facilitate measurements at small angles.

The first experiment, which we will refer to as the "low-resolution" setup, was incapable of distinguishing between elastic scattering and inelastic scattering involving excitation of nuclear levels within 10 MeV of the ground state. This setup was, however, designed for high precision, and it was suitable for measuring the small values of the ratio R which occur at small scattering angles. The inelastic scattering at such angles is a small fraction of the elastic scattering.

A second series of measurements was made with a "high-resolution" setup capable of resolving elastic scattering from much of the inelastic scattering which becomes important at large scattering angles. In this experiment, the momentum spread of the beam was reduced to $\pm 0.2\%$, and the scattered particles were detected with a multichannel detector located between the two spectrometer magnets at the place normally occupied by the momentum defining slits. The beam was monitored and positioned with the usual ion chambers, which were behind the targets. Cycling between right and left scattering angles was not done since, at the large angles, small changes in beam angle do not produce important errors. The Faraday cup was used only once to calibrate the ion chambers. In general, the high-resolution setup was designed to measure fairly large values of R in the presence of appreciable inelastic scattering, with somewhat reduced precision.

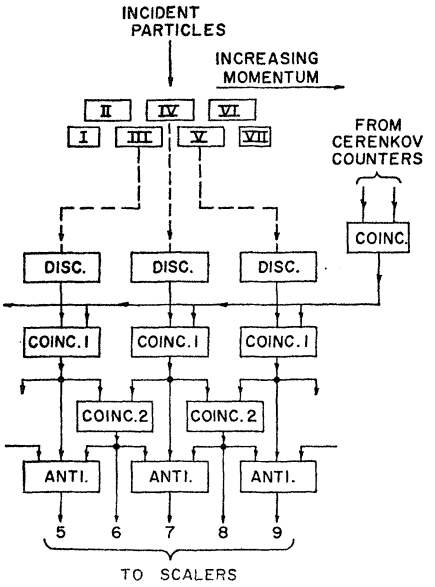

FIG. 3. Schematic view of the multichannel detector and partial block diagram of the electronics. The "ladder" counters I–VII are shown in cross section. The coincidence circuits "Coinc. 1" require that all particles recorded have also been detected in both of the Čerenkov counters which back up the multichannel ladder. The outputs of the circuits "Coinc. 2" represent counts in the channels defined by the overlap of the ladder counters. In the "Anti." circuits, "Coinc. 1" outputs are vetoed by either of the neighboring "Coinc. 2" outputs. The "Anti." outputs thus represent counts defined by the central regions of the ladder counters. The outputs of the "Coinc. 1" circuits are also monitored by scalers to provide a check. If the electronics is working properly, the counts recorded from "Coinc. 1" associated with counter IV, for example, must equal the sum of final outputs 6, 7, and 8.

The multichannel detector is shown in cross section in Fig. 3. It consisted of a "ladder" of seven overlapping scintillators, each of which was $\frac{1}{4}$ in.$\times\frac{3}{4}$ in. in cross section and $3\frac{3}{4}$ in. long. These were backed up by a telescope consisting of two Lucite Čerenkov counters, each 2 in. thick. The other Čerenkov counter dimensions, $4\frac{1}{2}$ in.$\times 4\frac{1}{2}$ in. for the first counter and 5 in. $\times 6$ in. for the second, ensured that any positron or electron from the target which passed through the ladder would be counted. It was necessary to require a threefold coincidence between the ladder and two Čerenkov counters in order to reduce the background, since the shielding at the location of the ladder was quite poor.

Figure 3 also shows a block diagram of the electronics used to convert information from the seven ladder counters into counts in 13 momentum channels. The channel width of $\frac{1}{4}$ in. corresponds to a momentum spread $\Delta p/p = 0.32\%$. This arrangement facilitates high-precision comparisons of cross sections. In a conventional ladder with 13 scintillators $\frac{1}{4}$ in. wide, edge effects would make it difficult to maintain highly stable counter efficiencies. In our case, every particle passing through the ladder must produce a full-sized pulse in at least one counter. Provided that the electronics works correctly, one and only one count will be recorded for each particle passing through the ladder. Edge effects only influence which of two neighboring channels will record a count. Thus, if an integration over several channels is performed to determine a cross section, the edge effect is the same as that for a single counter as wide as the integration region.

Figure 4 shows electron data from bismuth taken at 30°, 302 MeV with the ladder. (The 2 μC unit of beam intensity refers to charge collected by an ion chamber with gas gain ≈ 35.) Six sets of points are shown, constituting two groups of three. One group was recorded before and the other after the positron data were taken. Each group consists of points recorded with the elastic peak at three different parts of the ladder, i.e., at three different spectrometer field settings. No normalization has been used to correct for varying counter efficiencies.

The horizontal scatter indicates the precision with which the beam momentum was set. The width of the peak illustrates the resolution of the experiment, since inelastic scattering is small at this angle. The resolution is somewhat poorer than that achieved in similar electron scattering experiments, and this is due primarily to the target thickness and incident energy spread chosen. Since the positron beam intensity is about 10^{-4} of the electron beam intensity, it has been necessary to sacrifice some resolution in order to obtain useful counting rates.

DATA, CORRECTIONS, AND UNCERTAINTIES

Low-Resolution Experiment

The procedure for the low-resolution experiment was that described in Ref. 13. The target thickness for bismuth was 0.216 g/cm^2; for cobalt, it was 0.456 g/cm^2, except at 40°, where it was 3 times that thickness. The targets used in both experiments were in the form of thin metal sheets; a spectrographic analysis indicated the following impurities: for Co(0.2% Si, 0.1% Mn, 0.02% Al, 0.5% Ni, 0.01% Cu); for Bi(0.002% Al, 0.004% Pb, 0.001% Cu, 0.002% Ag). These do not represent a contamination of enough significance to influence our results. The energy was 302±2 MeV. The low-resolution data, including the main corrections and uncertainties, are summarized in Table I. Measured values of R, after small corrections for scaler dead time and for background have been made, are designated by R_0 and are given in column 3. Final values and uncertainties, R_f and ϵ_F, are given in columns 12 and 13.

The angle correction δ_θ is zero to first order, since data from right and left scattering of both positrons and electrons were averaged. At very small angles, however, the cross section varies so rapidly with angle that a correction was necessary. This correction was easily calculated from the measured left-right asymmetries.

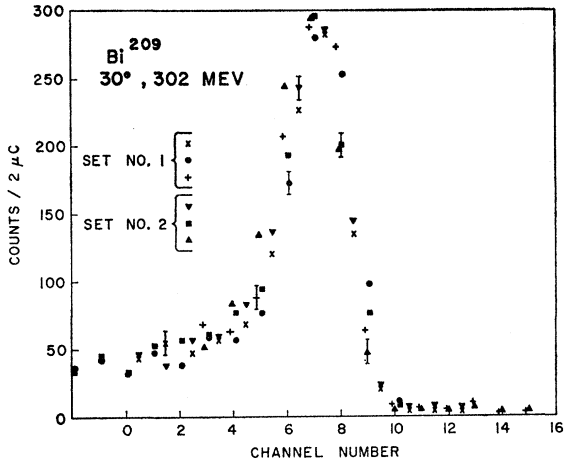

FIG. 4. Spectrum of 302 MeV electrons scattered at 30° by Bi^{209}. Six types of points are shown corresponding to 2 sets of data, each at three different spectrometer fields. The two sets were taken many hours apart. A few representative statistical errors are shown.

The energy correction δ_E results from the fact that two independent energy measurements were made. The measured counting rate as a function of spectrometer field gives one determination of the incident energy, while the field in the beam-analyzing magnet at the end of the accelerator provides another. The energy difference is inferred from the weighted average of the two measurements.

The uncertainties ϵ_θ and ϵ_E given in Table I, reflect the precision with which the angle and energy corrections could be made. The quantity ϵ_r indicates the accuracy of the correction for scaler dead time, while ϵ_M is the uncertainty in monitoring the beam. The net instrumental uncertainty from these sources ϵ_{inst} has been combined with the statistical error to arrive at the final error ϵ_F. A more detailed discussion of the instru-

TABLE I. Low-resolution data. R_0 is the measured ratio after small corrections for scaler dead time and background have been applied. The corrections δ_θ and δ_E arise from small known differences in the energies and scattering angles at which positron and electron data were taken. Uncertainties in these quantities lead to the errors ϵ_θ and ϵ_E, while ϵ_r and ϵ_M are, respectively, the error in making the scaler dead time correction and the error in monitoring the beam. Columns 12 and 13 give the final ratio R_F and its standard error ϵ_F. This last quantity was obtained from the net instrumental and statistical errors ϵ_{inst} and ϵ_{stat}. Column 14 lists the fraction of the electrons which are estimated to have been scattered inelastically.

1	2	3	4	5	6	7	8	9	10	11	12	13	14
Target	Angle	R_0	δ_θ	δ_E	ϵ_θ	ϵ_E	ϵ_r	ϵ_M	ϵ_{inst}	ϵ_{stat}	R_F	ϵ_F	Inelastic contamination (f)
Co^{59}	10°	+0.015	···	+0.002	±0.001	±0.002	±0.003	±0.002	±0.005	±0.005	+0.017	±0.007	<0.003
Co^{59}	20°	−0.047	···	+0.010	±0.001	±0.004	±0.003	±0.002	±0.006	±0.006	−0.038	±0.008	<0.035
Co^{59}	30°	−0.211	···	+0.010	±0.001	±0.006	±0.001	±0.002	±0.007	±0.010	−0.205	±0.011	0.17 ±0.04
Co^{59}	40°	−0.28	···	···	±0.001	±0.002	···	±0.004	±0.005	±0.050	−0.28	±0.051	0.62 ±0.12
Bi^{209}	5°	+0.017	−0.008	−0.006	±0.002	±0.001	±0.005	±0.004	±0.007	±0.004	+0.003	+0.008	<0.002
Bi^{209}	10°	+0.009	−0.001	−0.008	±0.001	±0.002	±0.002	±0.003	±0.004	±0.005	+0.000	±0.006	<0.003
Bi^{209}	15°	−0.011	···	−0.010	±0.001	±0.003	±0.001	±0.004	±0.006	±0.008	−0.021	±0.010	<0.006
Bi^{209}	20°	−0.182	···	−0.007	±0.001	±0.005	±0.002	±0.002	±0.006	±0.005	−0.183	±0.008	<0.04
Bi^{209}	30°	+0.051	···	−0.009	±0.001	±0.003	···	±0.002	±0.005	±0.018	+0.044	±0.019	0.072±0.017
Bi^{209}	45°	−0.41	···	−0.004	±0.001	±0.012	···	±0.004	±0.013	±0.012	−0.41	±0.12	0.31 ±0.07

mental errors in the low-resolution experiment has been given in Ref. 13.

The radiative corrections to the elastic scattering are about 8% for the low resolution data, and about 15% for the high resolution data discussed below. However, the corrections for positrons and electrons are so closely identical that they produce no significant change in R.[14]

Column 14 of Table I lists the fraction of the electrons detected which are estimated to have been inelastically scattered. High-resolution measurements at 300 MeV have been made by Kendall[7] for cobalt at 31° and 40° and for bismuth at 31° and 45°. From these data and from the known momentum resolution of the low-resolution experiment, the inelastic contamination for electrons at the large-angle points was directly calculated. At the smaller angle points, limits on the contamination have been found by extrapolation, assuming a dependence on momentum transfer characteristic of $E2$ transitions for cobalt and $E3$ transitions for bismuth. These correspond to the respective lowest order electric multipole transitions which make significant contributions to the scattering. Since the relative importance of the low-order transitions increases with decreasing angle under the present conditions, this procedure leads to an upper limit of the contamination at the small angle points. The $E1$ transitions which lead to the "giant resonance" are ineffectual since their excitation energies place them mostly out of the range of energies accepted by the spectrometer. Furthermore, their form factor[15] is proportional to the form factor for elastic scattering. The proportionality factor is $\frac{1}{8}(\hbar^2\Delta^2/\mu)(1/\hbar\omega)$, where $\hbar\omega$ is the energy of the giant resonance level, Δ is the momentum transfer, and μ is given by $\mu=\frac{1}{4}Am$ in which A is the atomic number and m the mass of the nucleon. For cobalt and bismuth at small angles under our conditions, this factor is <0.01.

In the case of bismuth, it is conceivable that an $E2$ transition, too small to be identified at large momentum transfers, might become important at the lower momentum transfers of the small-angle points. However, no such level is known in this element.[16]

We have assumed, as in Ref. 6, that magnetic transitions are not important. The expressions for the inelastic cross sections given in that reference, in the first Born approximation, have been used in our estimates.

Before inelastic positron scattering data became available, the inelastic contribution to R could not be properly subtracted out; and, thus, the usefulness of the large-angle data of the low-resolution experiment was limited.

[14] Only the effect of radiation by the recoil nucleus gives rise to a difference in the corrections for positrons and electrons. From the formulas of Tsai [Phys. Rev. **122**, 1905 (1961)], this difference is negligible for this experiment.

[15] J. Goldemberg, Y. Torizuka, W. C. Barber, and J. D. Walecka, Nucl. Phys. **43**, 242 (1963).

[16] *Nuclear Data Sheets*, compiled by K. Way *et al.* (Printing and Publishing Office, National Academy of Sciences–National Research Council, Washington 25, D. C.).

High-Resolution Experiment

Data in the high-resolution experiment were taken with the multichannel detector in the following way:

(1) An x-ray picture of the electron beam was taken to check its shape.
(2) The spectrometer field was set for 302 MeV/c.
(3) The beam energy was adjusted so that the elastic peak fell at the center of the ladder.
(4) Data were taken at this spectrometer field and also at settings above and below this field, to average any irregularities of the ladder.
(5) Steps 1–4 were repeated for various angles.
(6) Steps 1–5 were repeated for positrons.
(7) Steps 1–5 were repeated for electrons.
(8) At intervals of several hours, the counters and electronics were tested by measuring the scattering of electrons or positrons by a $\frac{1}{4}$-in.-thick copper target at a *scattered* energy of 250 MeV. Under these conditions, the scattered spectrum is fairly flat; and variations in counter efficiency are reflected in the counting rates of the 13 channels.

The target thicknesses in the high-resolution experiment were 0.916 g/cm^2 for cobalt and 0.531 g/cm^2 for bismuth. The energy was 302±1 MeV.

In determining R, the total number of counts in the elastic peak was found by adding the counts recorded in the region extending upward from a cutoff, 3 MeV below the peak. The error assigned to the total was the statistical error combined with an error corresponding to an uncertainty of ±0.25 MeV in the location of the cutoff. This added error takes into account fluctuations in the fields of the spectrometer and of the beam-analyzing magnet, and also possible biases in the way points next to the cutoff were included in the summation. The error in R due to these causes is labeled ϵ_0, and it is given in column 6 of Table II.

Table II also gives both the angle error ϵ_θ based on an estimated reproducibility of the scattering angle of ±0.03°, and the energy error ϵ_E calculated for an energy reproducibility of ±0.2%. In estimating ϵ_{eff}, the error in R arising from changes in counter efficiency, we have assumed that for a "set" of data (item 4 in the procedure outlined above), fluctuations of the mean counter efficiency have a standard deviation of 1.5%. This is based on a large number of checks with statistical accuracies of 2% or better, using the thick copper target (item 8 of the above procedure). No random or secular changes in efficiency were observed outside of those expected from statistics. In addition, the 30° electron data, taken on three runs widely spaced in time, reproduced in absolute value to within statistical errors of ±2%. (The remaining data were also consistent within statistics).

Remaining errors not listed in Table II are a beam monitor error of ±0.005 for all determinations of R, and an error of ±0.005 for all bismuth points arising

TABLE II. High-resolution data. Columns 3 and 8 give the final ratio R_F and its standard error ϵ_F. The errors arising from uncertainties in beam angle and energy are designated by ϵ_θ and ϵ_E. The statistical error, combined with the error resulting from an uncertainty of ±0.25 MeV in the location of the low-energy cutoff used in finding the area under the elastic peak, is given by ϵ_0, while ϵ_{eff} is an estimate of the error in R_F due to changes in counter efficiency. Column 9 gives the inelastic contamination estimated to be still present in the elastic scattering data; and column 10 gives the ratio R_{in} for inelastic scattering.

1	2	3	4	5	6	7	8	9	10
Target	Angle	R_F	ϵ_θ	ϵ_E	ϵ_0	ϵ_{eff}	ϵ_F	Inelastic contamination (f)	R_{in}
Co^{59}	30°	−0.206	±0.005	±0.014	±0.016	±0.006	±0.023	0.13	−0.014±0.03
Co^{59}	35°	−0.337	±0.007	±0.014	±0.034	±0.009	±0.037	0.19	−0.011±0.05
Co^{59}	40°	−0.028	···	···	±0.051	±0.006	±0.052	0.19	−0.012±0.08
Co^{59}	45°	+0.143	···	···	±0.07	±0.009	±0.071	0.05	+0.07 ±0.17
Bi^{209}	30°	+0.045	±0.003	±0.01	±0.013	±0.006	±0.019	0.03	+0.05 ±0.03
Bi^{209}	35°	−0.160	···	±0.01	±0.033	±0.009	±0.035	0.03	−0.03 ±0.06
Bi^{209}	40°	−0.394	···	±0.01	±0.057	±0.009	±0.059	0.03	−0.05 ±0.12
Bi^{209}	45°	−0.035	···	±0.01	±0.08	±0.009	±0.081	0.05	+0.07 ±0.13

from nonuniformity in the target thickness. Only one correction has been made: R was decreased by 0.004 to account for positron annihilation in the counters. The final values and uncertainties, R_F and ϵ_F, are given, respectively, in columns 3 and 8 of the table.

The resolution used in this experiment was not sufficient to eliminate entirely the contribution of inelastic scattering to the measured ratios. The known levels at 1.3 MeV ($E2$) for Co^{59} and at 2.6 MeV ($E3$) for Bi^{209} are inside the cutoff used in summing the elastic peak. Estimates of these contaminations were made following the procedure outlined in the discussion of the low-resolution experiment, and the fractional contaminations are given in column 9 of Table II.

Figure 5 shows complete spectra obtained for electrons and positrons scattered from cobalt at angles of 35°, 40°, and 45°. Close examination of this figure shows that the inelastic parts of the spectra behave somewhat differently from the elastic peaks for positrons and for electrons. Many levels contribute to the inelastic scattering seen in the figure. While some of the more prominent of these levels have been identified in very high-resolution electron scattering experiments,[6] none are well resolved here. For this reason, we have summed the inelastic data up to a cutoff 3.5 MeV below the elastic peak, subtracted the radiative tail of the elastic scattering, and derived from the result a ratio for inelastic scattering R_{in}, defined in the same way as R for elastic scattering. Values of R_{in} are given in column 10 of Table II with the associated, mainly statistical, errors.

The inelastic ratio lumps together the contributions of all of the levels responsible for inelastic scattering in the region below the cutoff. Nevertheless, within the large errors assigned, R_{in} agrees with values obtained by summing only small regions around the 3.95-MeV levels in cobalt and the 4.3-MeV level in bismuth. These are the most prominent levels for these elements in the region below the cutoff.

DISCUSSION

The elastic scattering ratios are shown in Figs. 6 and 7. The high-resolution data are as listed in Table II. The large-angle, low-resolution, data of Table I have been corrected for the effects of inelastic contamination, using R_{in} as determined in the high-resolution experiment. The inelastic ratio is the average ratio for an energy range which closely corresponds to that of the inelastic contamination in the low-resolution experiment. The corrected values of R shown in the figure are given by

$$R=\frac{1-r-f(1-r_{\text{in}})}{1+r-f(1+r_{\text{in}})}, \tag{2}$$

where

$$r=(1-R_0)/(1+R_0),$$

with $R_0\equiv R_F$ of Table I; and

$$r_{\text{in}}=(1-R_{\text{in}})/(1+R_{\text{in}}),$$

with R_{in} as given in Table II. The parameter f is the inelastic contamination given in Table I. Statistical

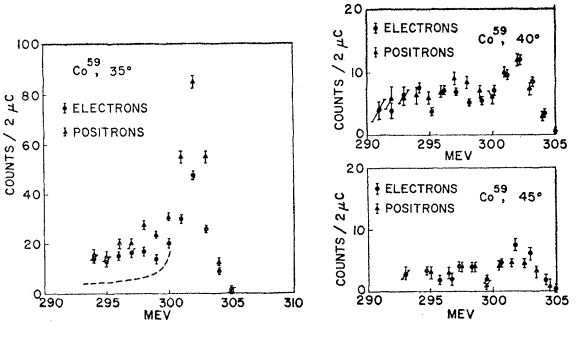

FIG. 5. Spectra obtained for electron and positron scattering by cobalt at 35°, 40°, and 45°. The data include elastic and inelastic components of the scattering, as well as the radiative tail which is shown for the 35° electron data by a dashed line.

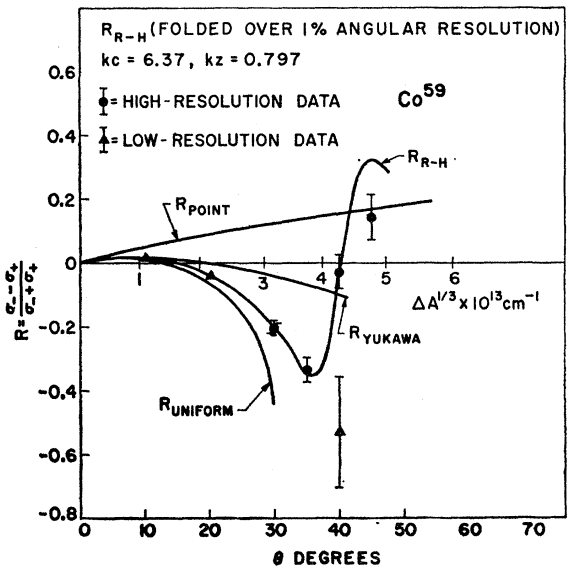

FIG. 6. The ratio R for Co^{59} at 302 MeV. The curves represent theoretical predictions: R_{point}, R_{Yukawa}, and $R_{uniform}$ are calculated in the second Born approximation; R_{R-H} is the phase-shift calculation of Herman, Clark, and Ravenhall, folded over ±1°angular resolution.

errors have been propagated through Eq. (2) to establish the error in R.

The curves labeled R_{point}, R_{Yukawa}, and $R_{uniform}$ in Figs. 6 and 7 are calculated from the second Born

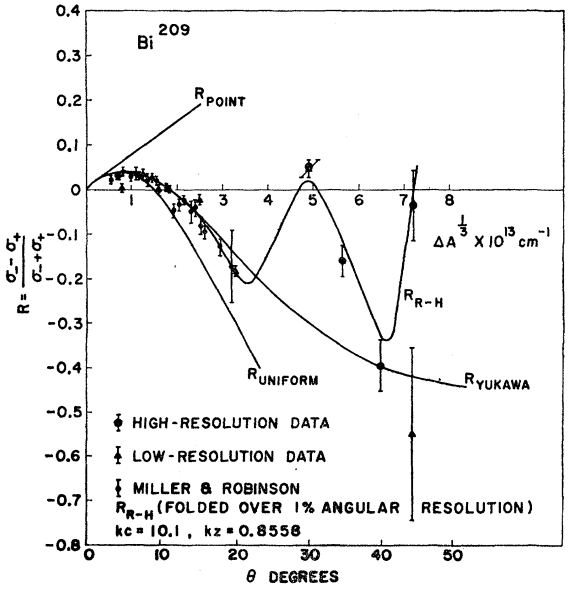

FIG. 7. The ratio R for Bi^{209} at 302 MeV. The curves represent theoretical predictions: R_{point}, R_{Yukawa}, $R_{uniform}$ are calculated in the second Born approximation; R_{R-H} is the phase-shift calculation of Herman, Clark, and Ravenhall. Also shown are the experimental points of Miller and Robinson taken at lower energies and scaled according to Eq. (3).

approximation formulas given by McKinley and Feshbach,[17] Lewis,[18] and Drell and Pratt.[19]

The curves labeled R_{R-H} represent results of phase-shift calculations by Herman, Clark, and Ravenhall.[3] The calculations were done for an energy of 300 MeV, using the Fermi model charge distribution, $\rho(r)=\rho_0/\{\exp[(r-c)/z]+1\}$, and were folded over a ±1° angular resolution. The parameter c characterizes the nuclear radius, while z characterizes the surface thickness. (The surface thickness t is the radial distance in which the charge density changes from 10 to 90% of its peak value; $t=4.40z$ for this model.) The values of the parameters were chosen to fit the electron scattering data of Ref. 4: For cobalt, $kc=6.37$, $kz=0.797$; for bismuth, $kc=10.1$, $kz=0.8558$ (see Ref. 3); $k=E/\hbar c$.

Looking first at the smaller angles, the cobalt data behave in the expected way. The data appear to be consistent with the second Born approximation for a reasonable model, i.e., they are midway between the predictions for the Yukawa and uniform charge distributions. At 10°, the second Born approximation is nearly model-independent, and the predictions and data agree.

The bismuth data at 5° and 15° do not appear to be consistent with the second Born calculations shown. Drell and Pratt[19] have derived a result which enables us to compare our data on bismuth with the data of Miller and Robinson[8] on lead taken at energies between 48 and 170 MeV at angles ranging from 21° to 74°. Drell and Pratt show that, in the second Born approximation, at angles which are small in absolute value and also small compared with the angle at which the first Born approximation has its first zero, R is given by

$$R=Z\alpha G(\Delta)/E, \tag{3}$$

where $G(\Delta)$ is a function only of the momentum transfer Δ, and α is the fine structure constant. The form of G depends on the nuclear charge distribution; but the relation permits a model-independent scaling law, at least for single-parameter models such as the uniform and Yukawa models shown here. The transformed data of Miller and Robinson are also shown in Fig. 7, and these data are consistent with the predictions of the second Born approximation.

Several possibilities are suggested by the foregoing comparison: The two experiments may be inconsistent; the transformation may not be valid for high-Z elements for the range of angles and energies over which it has been applied; the predictions of the second Born approximation which are shown may not be valid even at small angles, for the high-Z elements and high energies involved here.

Turning now to the large-angle data, the predicted oscillatory behavior of R is well verified. The positron

[17] W. A. McKinley, Jr., and H. Feshbach, Phys. Rev. **74**, 1759 (1948).
[18] R. R. Lewis, Phys. Rev. **102**, 537 (1956).
[19] S. D. Drell and R. H. Pratt, Phys. Rev. **125**, 1394 (1962).

and electron cross sections may also be seen to differ greatly in some instances. (A value of $R=0.33$ corresponds to a factor of 2 in the ratio of the cross sections.) The second Born approximation is seen to fail rather completely for $\Delta A^{1/3} \gtrsim 3.5$, i.e., after the start of the first diffraction dip in the first Born approximation. And the amplitudes of the oscillations of R are at least as great for cobalt as for bismuth, in spite of the difference in atomic number. This reflects the greater sharpness of the diffraction dips for cobalt.

We are prevented from drawing detailed conclusions from the large-angle data by several unanswered questions, both theoretical and experimental in origin. The major experimental question is the inconsistency of the 40° cobalt and 45° bismuth data at high and at low resolution. The discrepancy was discovered during the high-resolution experiment, with the result that these data were repeated and a thorough (though unsuccessful) search was made for hidden instrumental errors. On the other hand, the low-resolution data for the two targets were taken quite independently and were separated in time by several months, so that a single gross error cannot be blamed. The most plausible assumption seems to be that the low-resolution, large-angle data were taken at angles around 2° smaller than those of the high-resolution experiment; but, from known factors, we estimate 1° as the maximum angle difference possible.

A further experimental question arises from the inelastic contamination which could not be corrected for in the high-resolution experiment. Since this contamination is small, it is unlikely to lead to large errors; but some uncertainty from this cause must be assumed. If R were close to zero for this contamination, the cobalt data at 30° and 35° would be shifted in R by about -0.03 and -0.06, respectively. The other data would not be significantly affected.

Another question, previously ignored, is the validity of any pure potential scattering calculation for R. If "dispersive" scattering is important, e.g., scattering in which the exchange of two photons is accompanied by an intermediate excited state of the target nucleus, then R is directly sensitive to this effect. This has been discussed in connection with positron-proton scattering,[20] in terms of mesonic intermediate states or proton polarizability. Although dispersive effects in nuclear scattering are thought to be small in comparison with the total elastic cross section,[21] they may be large enough to affect the interpretation of R.

Finally, although the measurements of R_{in} are very crude, they indicate that this ratio is significantly smaller than the elastic ratio. Either this arises from cancellations in the average over many levels, or it indicates that scattering from the more prominent levels is better described by the first Born approximation than is the elastic scattering. The latter conclusion seems plausible experimentally; and it is supported by the fact that all of our data lie in a region away from the zeros of the first Born approximation expressions for the multipole orders known to be important (i.e., $E2$ and higher multipoles for cobalt and $E3$ and higher multipoles for bismuth).[6]

The work reported here best constitutes an exploratory effort. We hope, however, that further experimental work will be encouraged. It remains to be seen whether, in a practical sense, positron scattering represents an important adjunct to electron scattering in studies of nuclear structure.

The positron beam intensity available in these experiments was about 10^{-4} times the normal electron beam intensity. The construction of electron linacs with much larger beam power will make possible much more intense positron beams, even assuming no improvement in positron production efficiency. Thus, future measurements of R may simultaneously enjoy higher intensity and better energy resolution.

ACKNOWLEDGMENTS

We are especially indebted to H. Kendall, who made measurements of electron scattering from cobalt and bismuth for our use, and to R. Herman and D. G. Ravenhall for useful discussions.

In addition, we would like to acknowledge the support of Professor W. K. H. Panofsky and Professor W. C. Barber and the generous help of the linear accelerator personnel.

---

[20] See, for example, N. R. Werthamer and M. A. Ruderman Phys. Rev. **123**, 1005 (1961).

[21] A. Goldberg, Nuovo Cimento **20**, 1191 (1961); other references are given in this paper.